Research Article

Polymers and Polymer Composites

Polymers and Polymer Composites
Volume 32: 1–13

DOI: 10.1177/09673911241287889
journals.sagepub.com/home/ppc
Sage

The effect of modified titanium dioxide, silica, and zinc oxide on the self-cleaning property of an acrylic resin-based paint

Hoora Shahgolzade and Saeed Ostad Movahed

Abstract

Traffic paints hold paramount importance in road markings and ensuring efficient traffic flow. Self-cleaning marking traffic paints are a type of paint which recently developed to keep traffic lines clean with high visibility. Several paints were formulated with acrylic resin and self-cleaning agents, titanium dioxide (TiO2), silicon dioxide (SiO2), and zinc oxide (ZnO) individually and or in combination. All agents were treated in a furnace at 800°C for 2 hours before incorporating into the paint formulation. The effect of untreated and treated agents on several crucial properties of the formulated paints was assessed and compared. It revealed that heat treatment was effective on the crystallinity and impurity content of the agents evidenced by traditional characteristic techniques. The SEM-EDX analysis confirmed the presence and distribution of self-cleaning agents in the paint matrix. Water contact angles ranged from 68° to 97° for paints with self-cleaning agents, indicating improved hydrophilicity. Oil contact angles ranged from 27° to 42° for most paints with self-cleaning agents, showing some improvement in hydrophobicity. The qualitative assessment confirmed superior self-cleaning performance for paints with self-cleaning agents compared to the reference paint, especially for treated agents. Overall, the type and amount of self-cleaning agents significantly affect the hydrophilicity, hydrophobicity, and self-cleaning performance of paints.

Keywords

Marking paint, self-cleaning paint, acrylic resin, titanium dioxide, silicon dioxide, zinc oxide, heat treatment

Received 18 April 2024; accepted 13 September 2024

Introduction

Traffic paints hold paramount importance in road markings and ensuring efficient traffic flow.[1] Scientifically designed, these paints serve as essential tools in communicating regulatory information to drivers, pedestrians, and other road users. The application of traffic paints play a crucial role in enhancing road safety by clearly defining lanes, crosswalks, and signaling areas for controlled traffic movement.[2] Researchers emphasize the significance of durable formulations to withstand the impact of varying weather conditions and vehicular traffic. The retroreflective nature of traffic paints contributes to visibility during low-light conditions, significantly reducing the risk of accidents.[3] Ongoing scientific studies explore advancements in environmentally friendly formulations, addressing concerns related to ecological impact.[4] The applications of traffic paints also extend to parking lots, airport runways, and various transportation infrastructures, demonstrating their versatile role in urban planning and management. Rigorous scientific research in this field continues to refine traffic paint formulations, ensuring optimal performance and long-term effectiveness in maintaining organized and safe road networks.[5] Traffic paint is composed of a blend of materials designed to ensure safety and durability. Categorized into binders, pigments, fillers, additives, and retroreflective materials,[6,7] each component plays a key role in the overall composition. Binders function as the adhesive, effectively holding the various elements together and ensuring the paint adheres to the road surface. Commonly utilized binders include acrylic resins,[8] epoxy resins,[9] and chlorinated rubber.[10] Pigments contribute to the paint's coloration, with titanium dioxide being a prevalent choice for creating bright white lines that optimize visibility.[11] Iron oxide is another

Department of Chemistry, Faculty of Science, Ferdowsi University of Mashhad, Mashhad, Iran

Corresponding author:
Saeed Ostad Movahed, Department of Chemistry, Faculty of Science, Ferdowsi University of Mashhad, Mashhad 91886, Iran.
Email: s-ostad@um.ac.ir

major pigment responsible for yellow lines, often combined with titanium dioxide to enhance brightness. Additionally, carbon black is employed for black markings and symbols.[12] Fillers serve to bulk up the paint, improving its application and influencing properties such as texture and drying time. Common fillers encompass calcium carbonate, talc powder, and silica sand.[13] Additives play diverse roles, enhancing aspects like drying time, flexibility, and reflectivity. Examples include plasticizers, which increase paint flexibility and prevent cracking, crosslinking agents that improve paint adhesion and durability, and solvents for aid in the dissolution of other ingredients and adjust paint consistency.[14] Retroreflective materials are imperative for nighttime visibility, particularly through the incorporation of glass beads in the paint or pre-applied reflective tapes.[15] The specific combination of these ingredients is tailored to achieve desired properties, accounting for factors such as traffic volume, weather conditions, and budget constraints. Self-cleaning marking traffic paints are a type of paint which recently developed to keep traffic lines clean with high visibility.[16] The concept of self-cleaning traffic paints refers to early research dating back to the 1970s. However, significant advancements in materials and technology have developed in recent years. These paints have numerous advantages including, maintenance reduction, which leads to cost savings, and minimizes traffic disruptions, and pollution reduction which leads to cleaner roads reflecting more light, potentially improving nighttime visibility and reducing headlight glare. They also, benefited the environment through less frequent repainting resulting in lower solvent and paint usage, minimizing environmental impact.[17] Two main approaches dominate self-cleaning traffic paints:[18]

- Photocatalytic: These paints contain titanium dioxide (TiO2), which activates under UV light to break down dirt and organic matter. Rainwater then washes away the dirt, leaving lines clean and bright.
- Superhydrophobic: These paints create a surface where water moves up and rolls away, taking dirt and contaminants.

However, there are several challenges to the application of self-cleaning paints including, appropriate durability to ensure long-term performance and cost-effectiveness in real-world conditions. Also, currently, self-cleaning paints are more expensive than traditional options. Another challenge is the environmental impact. Some concerns exist regarding the potential release of titanium dioxide nanoparticles from photocatalytic paints. Despite these challenges, the potential benefits of self-cleaning traffic paints are undeniable. As research and development continue, someone can expect to see these innovative paints play a bigger role in keeping roads safer and more sustainable.[19–22]

Acrylic resins constitute a diverse class of polymers with versatile properties and applications.[23] These resins are formed through the addition polymerization of acrylic acid ($CH_2 = CHCOOH$) or its derivatives, such as methacrylic acid ($CH_2 = C(CH_3)COOH$) or acrylates/methacrylates (esters of these acids). Synthesized through bulk, solution, emulsion, or suspension polymerization methods, acrylic resins emerge as advantageous binders in the formulation of self-cleaning traffic paints.[24] Acrylic resins are renowned for their excellent durability against harsh weather conditions, including extreme temperatures, sunlight, and rain. This resilience is crucial for road markings, ensuring the sustained effectiveness of self-cleaning properties and reducing the frequency of repainting.[25] Forming a flexible film on the road surface, acrylic resins promote strong adhesion, preventing paint cracking or peeling. This characteristic is crucial for the proper functioning of the self-cleaning mechanism. Acrylic resins adhere effectively to various asphalt and concrete surfaces, establishing a secure bond that prevents paint from flaking off. This is essential for the visible traffic markings. Resistant to a range of chemicals, including de-icing salts and automotive fluids, make acrylic resins a priority to traditional paint binders. This resistance contributes to the long life of the paint in challenging environments. Some acrylic resins possess inherent self-cleaning properties due to their hydrophilic nature. When exposed to rain or dew, water droplets coalesce into larger ones and roll off the paint surface, carrying dirt away. Acrylic resins offer ease of application and maintenance, further enhancing their applications in traffic paint formulations. The environmental friendliness of acrylic resins adds to their eligibility to act as binders for self-cleaning traffic paints.[26]

In the self-cleaning traffic paints, the incorporation of titanium dioxide (TiO2), silicon dioxide (SiO2), and zinc oxide (ZnO) introduces distinctive advantages and drawbacks. Titanium dioxide exhibits excellent photocatalytic activity, engaging with UV light to destroy organic dirt and pollutants, thereby fostering a self-cleaning mechanism. Additional attributes include high brightness, reflectivity, durability, and weather resistance. Nevertheless, drawbacks encompass its relatively high cost, limited self-cleaning efficiency under low light conditions, and environmental considerations.[27] Silicon dioxide contributes to enhanced hydrophilicity, facilitating the creation of a water-attracting surface that prompts water droplets to amalgamate and roll off, carrying dirt away. This particle also augments paint durability and abrasion resistance, ensuring acceptable mechanical strength and protection against wear and tear. Nonetheless, challenges include low photocatalytic activity and the imperative need for the selection of SiO2 particle size and refractive index to mitigate adverse effects on reflectivity.[28] Zinc oxide emerges as a favorable component in self-cleaning traffic paint formulations, having moderate photocatalytic activity, antibacterial and antifungal properties, and cost-effectiveness. Nevertheless, it is marked by lower hydrophilicity and water repellency compared to SiO2, susceptibility to photodegradation, and potential environmental concerns.[29]

In ongoing research, efforts are directed toward exploring ways to combine these particles with each other and other materials or surface treatments (modification) to achieve synergistic effects and address existing limitations.[30–34] As an illustration, their effects on the properties of epoxy-based hybrid nano coatings were stidied.[35–39] This approach aims to optimize the benefits of each particle while mitigating their respective drawbacks, contributing to the continuous improvement of self-cleaning traffic paints. To do this, traditional titanium dioxide (TiO2), silicon dioxide (SiO2), and zinc oxide (ZnO) underwent treatment in a furnace at 800°C. Subsequently, various traffic paints were formulated, employing an acrylic resin and incorporating the aforementioned materials both before and after treatment, individually as well as in combination. The

structural alterations induced by the treatment were evaluated using standard techniques, specifically Fourier Transform Infrared Spectroscopy (FTIR) and X-ray Diffraction (XRD), providing insights into the modified characteristics of TiO2, SiO2, and ZnO. Additionally, the formulated paints underwent assessment of their self-cleaning parameters, with comprehensive measurements conducted and results recorded. The findings were thoroughly examined and discussed, emphasizing the impact of the treatment and material combinations on the structural and self-cleaning attributes of the traffic paints.

Experimental

Materials

Acrylic resin (STR-30T), a grade designed for marking paints binder, had a clear liquid with a glass transition temperature of +37°C, soluble in toluene, aromatic hydrocarbons, esters, ketones, and some aliphatic hydrocarbons but partially soluble in alcohols and glycols. It had a viscosity at 25°C (cP) (ASTM D-562) of 10,000-20,000 with a density at 25°C and flash point of 0.96 and 22°C, respectively. Titanium dioxide (TiO2, Anatase), pigment and self-cleaning agent with particle size between 0.4 and 12 μm supplied by Merck, Germany. Zinc oxide (ZnO), a self-cleaning agent with particle size less than 15 μm also supplied by Merck. Silica (SiO2.xH2O), a self-cleaning agent with particle sizes between 0.1 and 1 μm supplied by Riedel. Toluene and ethyl-methyl-ketone were used as solvents supplied by Merck. NACODISPER-2-2, a Solvent-free, low-dosage wetting, and dispersing additive, supplied by Noyan Afzon chem group, Iran.

Used identification techniques and self-cleaning assessments

Attenuated total reflectance Fourier transform infrared spectroscopy (ATR-FTIR) analysis was employed to investigate the chemical structure of both the prepared paints and the self-cleaning agents, titanium dioxide (TiO2), silicon dioxide (SiO2), and zinc oxide (ZnO). The ATR-FTIR analysis utilized an AVATAR 370FT-IR instrument from Termo Nicolet, USA, operating within a wavelength range of 300-4000 cm^{-1}. X-ray Diffraction (XRD) served as a non-destructive technique for qualitative and quantitative analysis of the crystalline materials.[40] In this study, the crystalline structure of the self-cleaning agents (TiO2, SiO2, and ZnO) was examined using an X-ray diffraction crystallography instrument from GNR, Italy. The analysis involved measuring the angles and intensities of diffracted beams within a range of 15 to 80° ($\lambda = 0.154$ nm), utilizing Cu Kα radiation at a tube voltage of 40 KV and a tube current of 30 mA. The detector employed was a Scintillator. The morphology of the paints was assessed using a field emission gun scanning electron microscope (SEM LEO 1450VP) from Germany, operating at 20 kV with a resolution of 2.5 nm. Elemental analysis of the samples was conducted using an energy-dispersive X-ray spectroscopy (EDX) instrument (7353, Oxford, UK) with a resolution of 133 eV. The SEM micrographs were concurrently studied to examine the shapes and morphology of the samples. The contact angle (θ) between water, automotive oil droplets (50 μL), and the paint surface was measured using a stereomicroscope (SZH10) equipped with a camera (Olympus DVP1) at a magnitude of 25x. It performed on a horizontal surface known as static contact angle. This comprehensive array of analytical techniques provided a detailed characterization of both the chemical and morphological features of the paints and self-cleaning agents.

The qualitative assessment of the self-cleaning property of the paints was conducted using carbon black and automotive oil as potential contaminants. Initially, a rectangular-shaped glass strip measuring 3 cm × 6 cm with a thickness of 4 mm underwent thorough washing with a traditional detergent, followed by complete drying. Subsequently, the glass strip's surface was coated with a thin layer of paint (200 μm) utilizing a laboratory equipment 4-side paint film applicator.[41] After allowing 24 h for the paint to dry at ambient temperature, the glass strip was positioned on a slope inclined at an angle of 20°. For the carbon black test, the paint surface received a thin layer of carbon black (*N*660, Pars Carbon Ltd, Saveh, Iran) at approximately 2.5phr. A droplet of water was then released onto the carbon black using a dropper, capturing and observing the rate of slipping, the extent of carbon absorption by water, and the removal of carbon black (contaminant) from the paint surface. The entire process was documented and observed using a D3200 Nikon camera. In the case of the automotive oil test, a single droplet of oil was applied to the paint surface, followed by the same procedure of water droplet application as in the previous test. The elimination of automotive oil from the paint surface was observed and recorded using the same camera setup as described above. This comprehensive testing methodology provided insights into the paints' ability to resist and eliminate contaminants, contributing to a qualitative understanding of their self-cleaning characteristics.

Sample preparation

The preparation of the formulated paints took place in a laboratory mechanical mixer (ADEB 56 *N*4, AEPHR, Germany). Initially, 100 parts per hundred (phr) of acrylic resin were placed inside a beaker and mixed with a solvent blend of toluene-methyl ethyl ketone (30phr-20phr) for 5 min at a speed of 1369 r/min. Following this, a dispersing agent (NACODISPER-2-2) was added, and the mixture underwent an additional 5 min of mixing. In the subsequent stage, the self-cleaning agents (TiO2, SiO2, ZnO, and/or their combinations) were introduced into the mixture, which underwent an additional 30 min of mixing. Subsequently, a 10-min ultrasound bathing process (CP104, Ceia, Germany) was employed to stabilize the paint formulation.

This systematic process ensured the thorough incorporation and stabilization of the self-cleaning agents within the acrylic resin-based paint.

The treatment and modification of self-cleaning agents, namely TiO2, SiO2, and ZnO, were executed at a temperature of 800°C for 2 hours utilizing a laboratory furnace (Kavosh Azma, Iran). Before their incorporation into the paint formulation, these agents underwent a pre-treatment process. Initially, they were wetted with methanol, then subjected to a 10-min ultrasound bath treatment (100 Hz), and subsequently dried at ambient temperature under a laboratory hood for 24 h. This process aimed at reducing particle sizes and enhancing the dispersion of the self-cleaning agents within the paint matrix. Table 1 represents the formulation of 12 prepared paints. In all samples, 100 phr acrylic acid, 2phr dispersing agent (NACODISPER-2-2), and 50phr solvent (toluene/methyl ethyl ketone, 3/2 wt ratio) were used. All values in phr. The symbol "m" refers to the treated self-cleaning agent.

Results and discussion

Modification of used self-cleaning agents

Titanium dioxide (TiO2). Figure 1 represents and compares the FT-IR spectra for self-cleaning agents, TiO2, SiO2, and ZnO before amendment and after amendment at 800°C for 2 hours. As observed, the modification was effective on all mentioned materials. The characteristic transmittance features observed in FT-IR spectra of TiO2 depend on several factors, including crystal structure, particle size and morphology, and impurities incorporated into the TiO2 network. TiO2 exists in three main polymorphs: rutile, anatase, and brookite. Each polymorph exhibits slightly different vibrational modes and therefore distinct peaks in the FT-IR spectrum. Also, smaller particles and certain morphologies can broaden or shift peaks due to confinement effects and surface interactions.[42] Ti-O stretching vibrations lay on 543 and 691 cm^{-1} , and 531 and 690 cm^{-1} for untreated and treated TiO2, respectively. The above-mentioned peaks are attributed to the anatase polymorph of the TiO2.[43] Another peak observes around 3100 cm^{-1} for untreated TiO2 which was attributed to the hydroxyl group (O-H) of water on the surface of sample. The absence of this peak in the treated sample is due to the evaporation of water inside the furnace. However, the intensities of TiO2 stretching vibration were higher for treated TiO2. The reasons refer to the following:

- Removal of surface contaminants: The treatment process might have removed impurities and hydroxyl groups (O-H) from the TiO2 surface. These species can dampen the Ti-O vibration signals through hydrogen bonding or by blocking access to the surface. Their removal in the treated sample could lead to a clearer and more intense signal for the Ti-O vibrations.
- Increased crystallinity amount: The treatment might have enhanced the crystallinity of the TiO2, particularly because it involved a heating step in the furnace. A more ordered crystalline structure can lead to sharper and more intense vibrational peaks compared to an amorphous or poorly crystalline material.
- Changes in particle size and morphology: The treatment altered the particle size or morphology of the TiO2, it could also affect the peak intensities. Smaller particles with larger surface areas can exhibit higher signal intensities due to increased interaction with the IR radiation. Additionally, certain morphologies might expose specific crystal planes more readily, leading to stronger signals for vibrations associated with those planes.

XRD patterns can be analyzed quantitatively to estimate crystallite size, phase abundance, and other parameters. The presence and relative intensity of specific peaks can determine whether the TiO2 sample is Anatase, Rutile, or a mixture of both. Also, sharp peaks indicate higher crystallinity, while broad peaks suggest smaller crystallite sizes or strain in the

Table 1. The formulation of the prepared paints. In all samples, 100 phr acrylic acid, 2phr dispersing agent (NACODISPER-2-2), and 50phr solvent (toluene/methyl ethyl ketone, 3/2 wt ratio) were used. All values in phr. The symbol "m" refers to the treated self-cleaning agent.

Sampe	TiO2	SiO2	ZnO	m-TiO2	m-SiO2	m-ZnO
1	10					
2		10				
3			10			
4				10		
5					10	
6						10
7	3.3	3.3	3.3			
8				3.3	3.3	3.3
9	5	2.5	2.5			
10				5	2.5	2.5
11	2.5	2.5	5			
12				2.5	2.5	5

material. If the peaks have different intensities from those expected for a random powder sample, it can indicate the preferred orientation of the crystallites. The theta (2θ) degrees in XRD patterns corresponding to Anatase and Rutile polymorphs of TiO2 are[44] 25.3°, 37.8°, 48.0°, 53.9°, 55.1°, and 62.7°; 27.4°, 36.1°, 41.2°, 54.5°, 62.9°, and 69.5°, respectively. The XRD patterns for self-cleaning agents, TiO2, SiO2, and ZnO before amendment and after amendment at 800°C for 2 hours were shown in Figure 2. As observed, all peaks corresponding with anatase polymorph were seen in the studied TiO2. In addition, two appeared peaks at 36.1 and 41.2° show the presence of a little Rutile polymorph in the structure of TiO2. However, the intensities of the peaks are lower for treated TiO2 compared with untreated TiO2. In the X-ray diffraction (XRD) patterns, the observed reduction in peak intensities for treated TiO2 compared to untreated TiO2 can be attributed to various potential reasons. The treatment process may have resulted in a reduction of crystallite size (not crystallite amount) or introduced strain

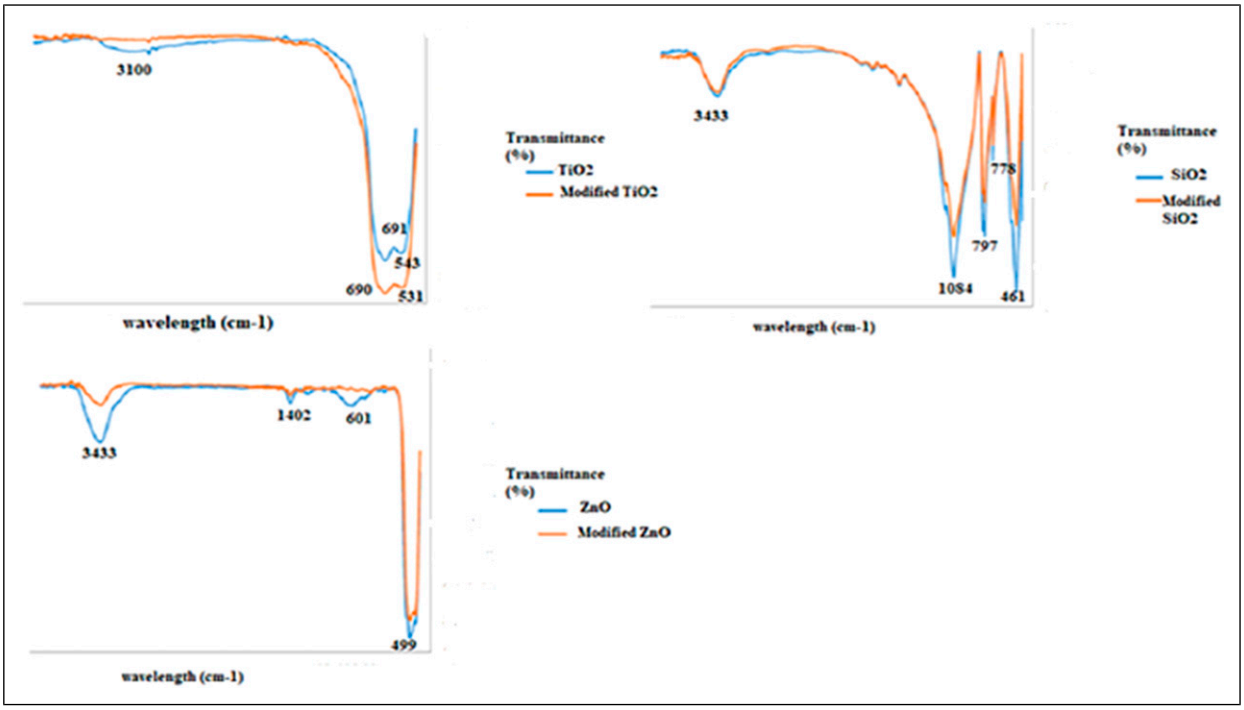

Figure 1. The FT-IR spectra for self-cleaning agents, TiO2, SiO2, and ZnO before amendment and after amendment at 800°C for 2 hours.

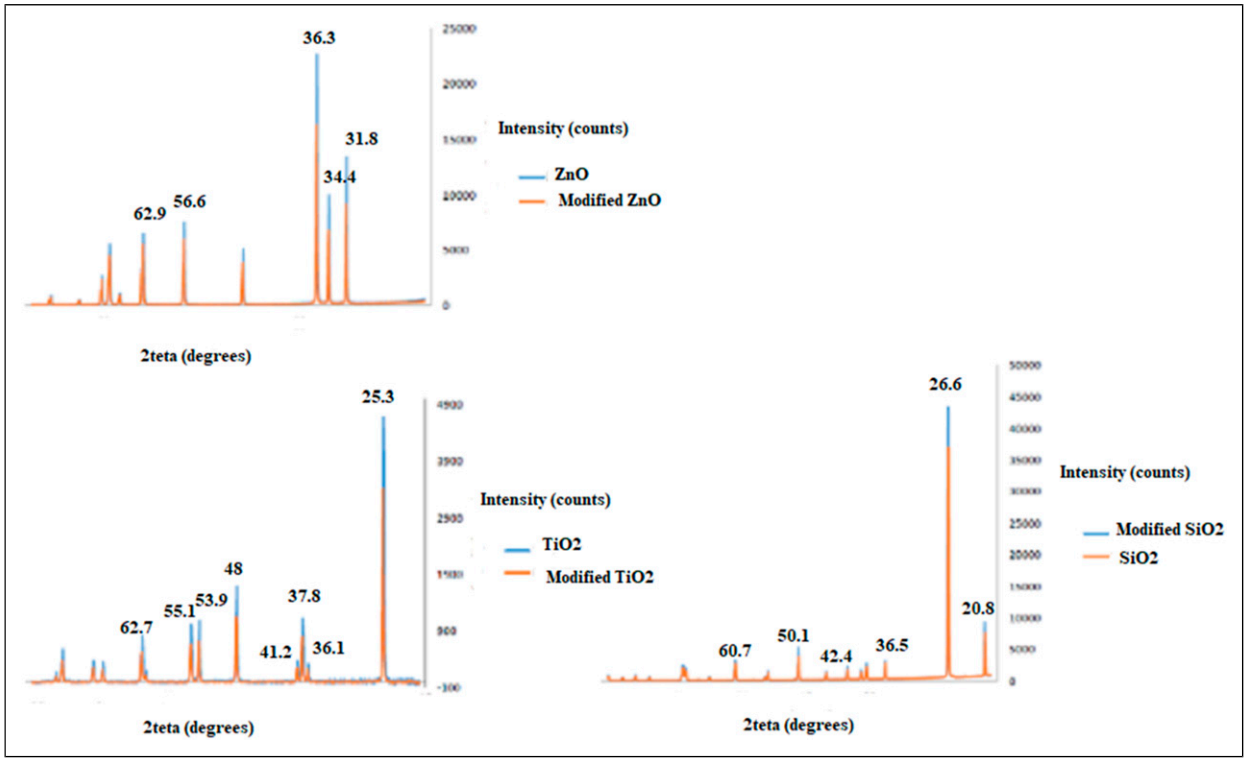

Figure 2. The XRD patterns for self-cleaning agents, TiO2, SiO2, and ZnO before amendment and after amendment at 800°C for 2 hours.

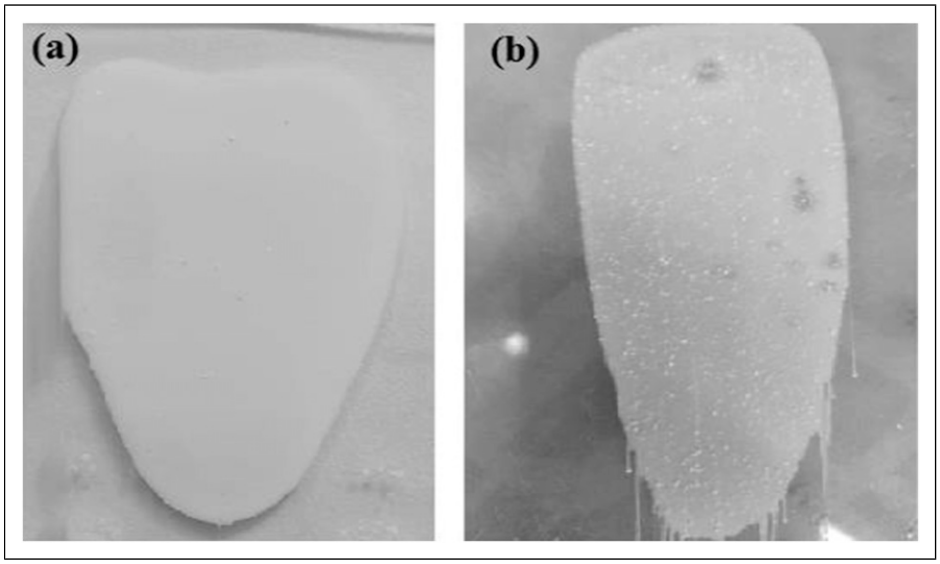

Figure 3. Unfavorable (b) and favorable (a) surface film formation for sample 1 (Table 1) after using optimal solvent value and ratio. The method for preparing the paints was explained in section 2-3 (Sample preparation).

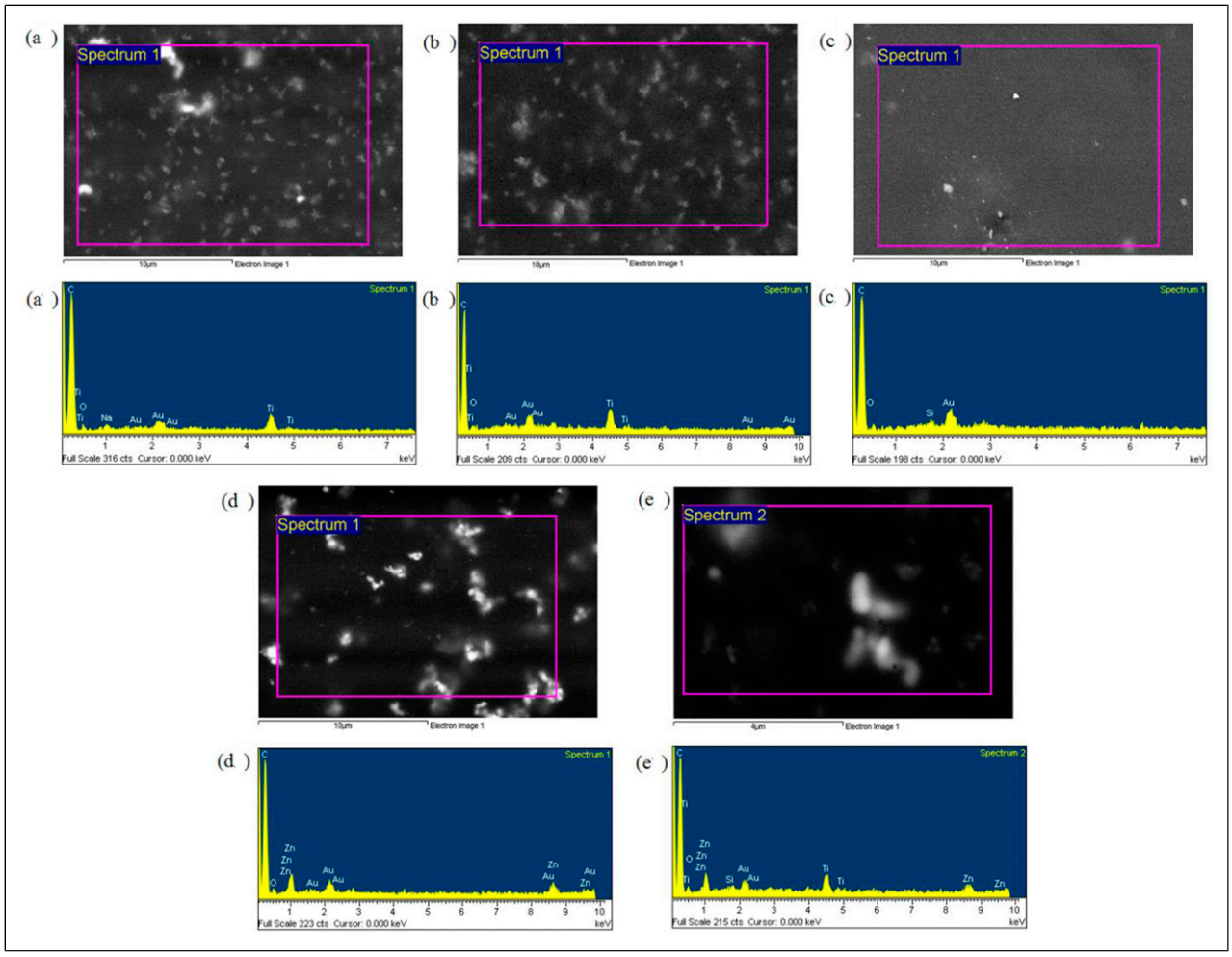

Figure 4. SEM-EDX images and spectra for samples 1, 4, 5, 6, and 10 as detailed in Table 1.

into the TiO2 structure. This phenomenon can lead to broader peaks with lower intensities, as less ordered crystalline domains exhibit decreased efficiency in diffracting X-rays. In addition, the treatment may have partially amorphized the TiO2 structure. Amorphous materials lack a well-defined crystal structure, resulting in the absence of sharp peaks in XRD patterns. This would lead to a significant decrease or even complete disappearance of characteristic Anatase peaks. The treatment might have

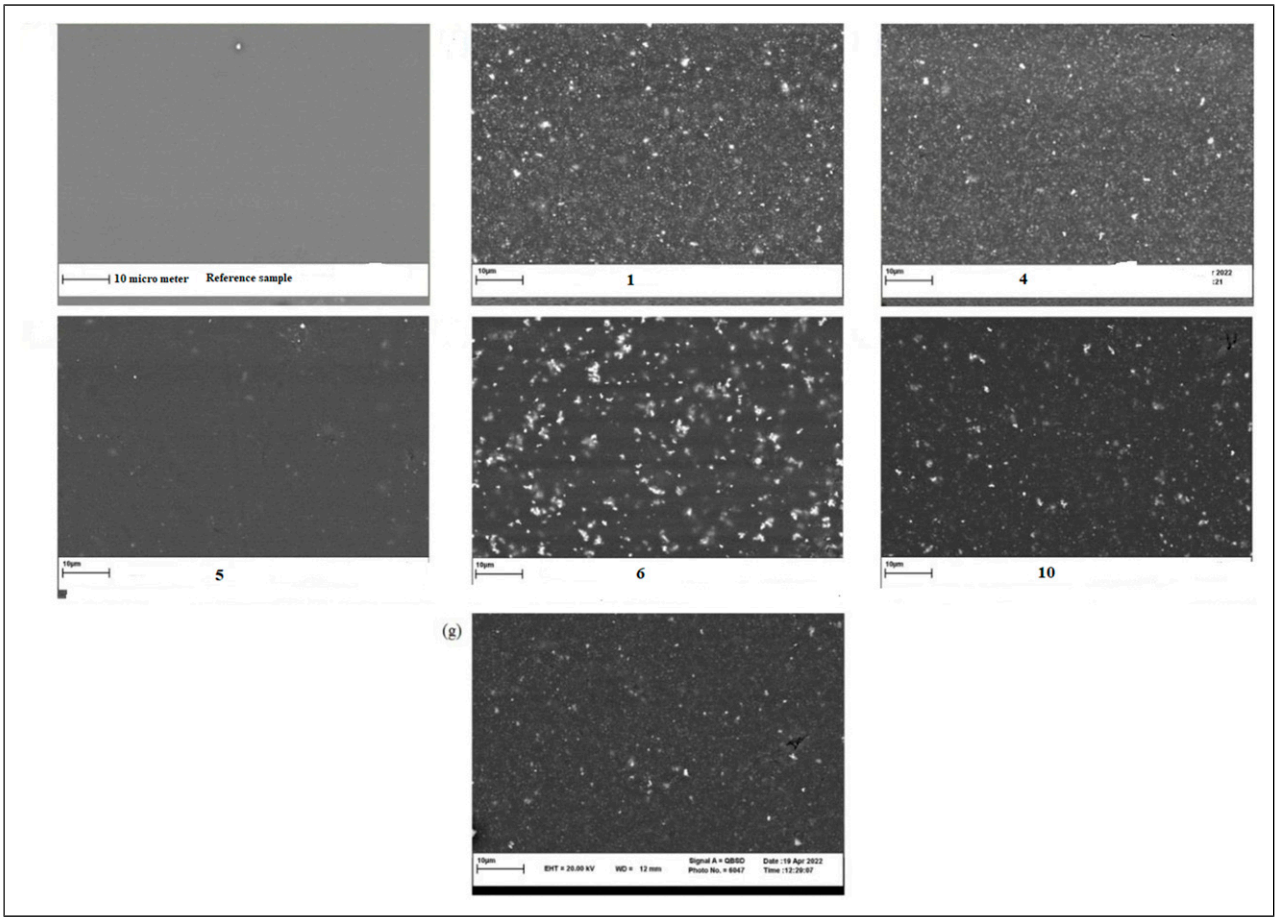

Figure 5. SEM images for samples 1, 4, 5, 6, 10, and reference (without a self-cleaning agent) as detailed in Table 1.

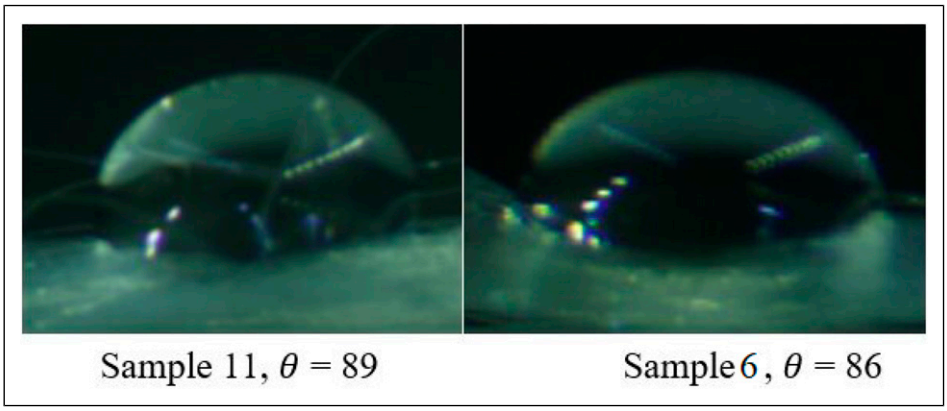

Figure 6. Typical contact angles (θ) between a droplet of water and formulated paints, Samples 11 and 6 (Table 1).

introduced a layer of amorphous material on the surface of TiO2 particles, acting as a barrier. This layer attenuates the X-rays reaching the crystalline core of the particles, thereby reducing the intensity of the diffracted peaks.

Silicon dioxide (SiO2). As observed from Figure 1, peaks in the FT-IR spectrum at 461, 1084, and 3433 cm^{-1} were attributed to Si-O bending, Si-O-Si asymmetric stretching, and O-H (in water) stretching vibrations, respectively.[45] Additionally, two more appeared peaks at 778 and 796 cm^{-1} were attributed to Si-O-Si symmetric stretching vibrations. However, after the treatment of silica (silicon dioxide) in a furnace at 800°C for 2 hours, the intensities of the above-mentioned peaks except for the hydroxyl group (O-H) decreased remarkably. The intensity reduction may refer to the formation of a new phase in silica structure. There is a possibility of partial transformation of the original silica phase into another polymorph like cristobalite or tridymite.[46] These different phases might have slightly different peak positions and intensities compared to the initial phase, affecting the overall spectrum. However, the O-H peak at 3433 cm^{-1} can be attributed to adsorbed and absorbed water

Table 2. Represents the contact angles (θ) between a droplet of water and automotive oil with formulated paints (Table 1). RC is a reference compound containing acrylic resin formulated without self-cleaning agents, TiO2, SiO2, and ZnO.

Sample	Contact angle (θ, *degree*) with water	Contact angle (θ, *degree*) with automotive oil
RC	100	33
1	88	27
2	97	31
3	93	29
4	77	30
5	87	33
6	86	32
7	93	32
8	96	42
9	95	31
10	68	27
11	89	27
12	100	23

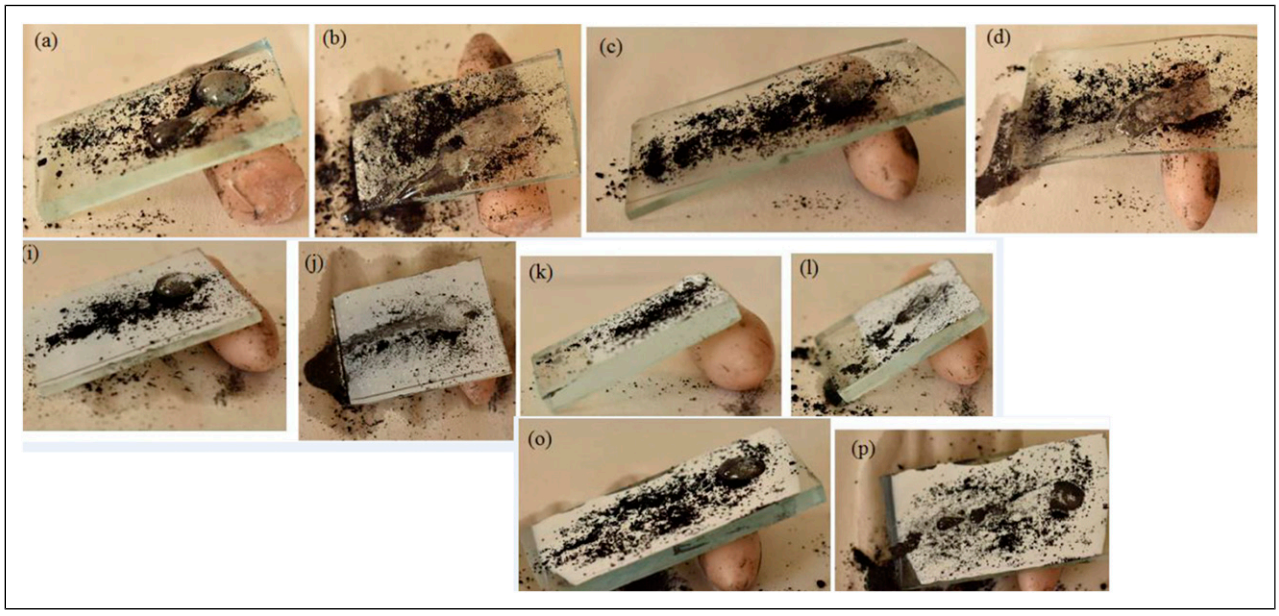

Figure 7. The qualitative self-cleaning characteristics of selected samples, denoted as RC (a and b), 2 (c and d), 8 (o and p), 10 (k and l), and 12 (l and j), as elaborated in Table 1, utilizing carbon black as potential contaminants. The images show the droplet position exactly after contact with the surface of paint and after a minute of contact.

molecules on the surface and in the structure of silica, respectively. At high temperatures, these water molecules can desorb from the silica surface, but as observed remain inside the silica leading to a slight decrease in the intensity of the O-H peak.

The theta (2θ) degrees corresponding to SiO2 in XRD patterns depend on its specific polymorph and morphology.[47] Figure 2 shows strong peaks at 20.8°, 26.6°, 36.5°, 42.4°, 50.1°, and 60.7°: These sharp peaks signify the ordered crystal structure of quartz, the most common crystalline form of SiO2. However, the intensities of the mentioned peaks increased after treatment.

The reason may refer to phase transformation after treatment. It seemed that SiO2 before treatment contained a mixture of SiO2 polymorphs, like a combination of amorphous and crystalline phases, the treatment could have triggered the transformation of the amorphous phase into the crystalline quartz form. Quartz exhibits much sharper and more intense peaks compared to other polymorphs or amorphous silicon dioxide, causing the observed increase. There is also another possibility. The treatment might have removed surface defects or impurities that were previously blocking X-rays from reaching the underlying crystalline structure. This improved access would lead to stronger peak intensities. Although less likely, the treatment could have caused the crystallites to align in a preferred orientation during recrystallization. This can lead to a "focusing" effect, concentrating X-rays on specific planes and further enhancing the intensities of those peaks.

Zinc oxide (ZnO). Figure 1 shows peaks in the FT-IR spectrum at 499, 601, 1402, and 3433 cm^{-1} were attributed to Zn-O bending, Zn-O stretching, C-O stretching (due to impurities in ZnO) and O-H (in water) stretching vibrations, respectively.[48] After treatment, corresponding peaks for water and impurities diminished resulting in water desorption and impurities

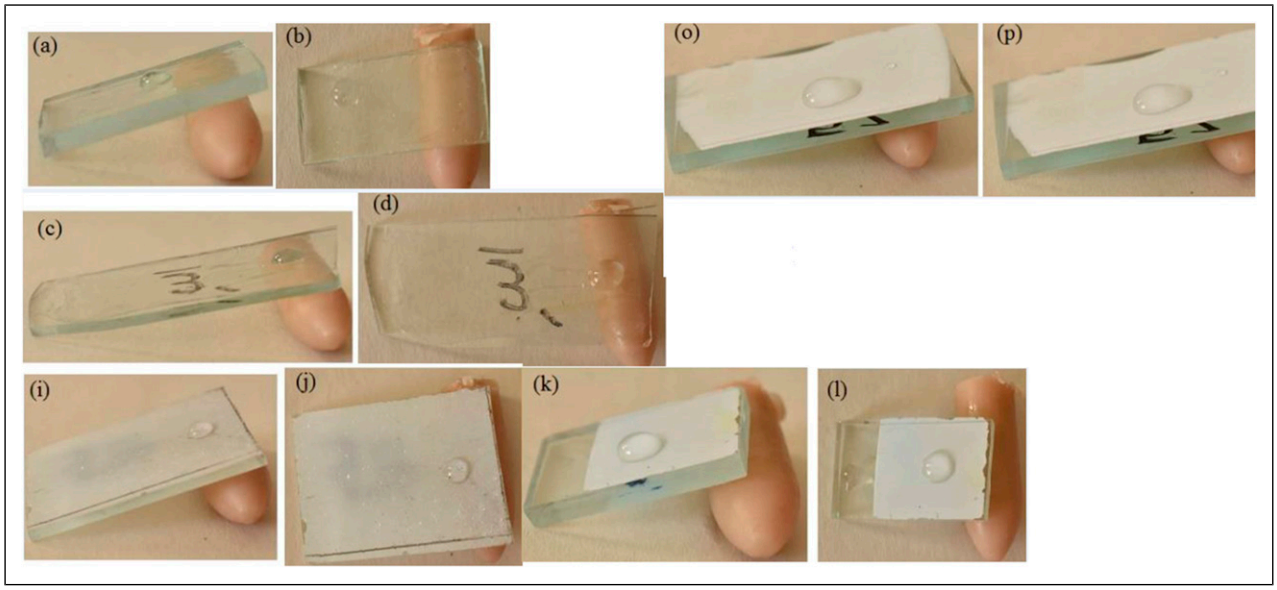

Figure 8. The qualitative self-cleaning characteristics of selected samples, denoted as RC (a and b), 2 (c and d), 8 (o and p), 10 (k and l), and 12 (l and j), as elaborated in Table 1, utilizing oil as potential contaminants. The images show the droplet position exactly after contact with the surface of paint and after a minute of contact.

degradation inside the furnace at 800°C. Also, the intensity of Zn-O vibrations, bending and stretching was reduced compared to untreated ZnO. High-temperature treatment can promote crystal growth and densification of the ZnO network. This leads to larger and more ordered crystalline domains, which might diffract the IR radiation more efficiently, affecting the transmission at the characteristic Zn-O vibrational frequencies. While the overall diffraction efficiency might increase, the direct interaction of IR radiation with individual Zn-O bonds inside the bulk crystalline structure might be less efficient compared to smaller crystallites or surface atoms. Also, the high temperature could potentially induce subtle changes in the local configuration of the Zn-O bonds. This could alter their vibrational modes and decrease the intensity of the characteristic peaks at 499 and 601 cm^{-1}. This is less likely compared to the other reasons but remains a possibility for specific treatment conditions and ZnO morphologies.

Figure 2 represents the strong peaks at 31.8°, 34.4°, 36.3°, 56.6°, and 62.9°. These sharp peaks signify the hexagonal wurtzite crystal structure, the most common form of ZnO.[49] As observed, after treatment inside the furnace at 800°C, the intensities of the above-mentioned peaks reduced. This conforms with FTIR findings. The crystal growth in treated ZnO might diffract X-rays differently compared to smaller crystallites in untreated ZnO. While larger and more perfect crystals can diffract X-rays more efficiently overall, the intensity of individual peaks can sometimes decrease due to changes in the way X-rays interact with the internal crystal structure. Although less likely, the high temperature could potentially have triggered partial amorphization of the ZnO, especially if the initial material contained a small amorphous fraction. Amorphous materials do not have a defined crystal structure and do not produce sharp peaks in XRD patterns, causing a decrease in peak intensity.

Characteristics of the formulated paints

Table 1 demonstrates the formulation of the prepared paints. As mentioned, in all samples, 100 phr acrylic acid, 2phr dispersing agent (NACODISPER-2-2), and 50phr solvent (toluene/methyl ethyl ketone, 3/2 wt ratio) were used. The optimal value and also the ratio of toluene to methyl ethyl ketone were assessed by the qualitative assessment of paint viscosity as described earlier with a 5-s falling time. The type and amount of solvent used significantly affected the paint's viscosity, influencing its flow, application ease, and leveling properties. Thicker paints with less solvent might require thinning for brush application, while paints with high solvent content might be thinner and spray better. Finding the right balance is crucial for ensuring the paint applies smoothly and evenly on different surfaces. In addition, after application, the solvent evaporates, allowing the binder (often a polymer) to form a continuous film that adheres to the substrate. This film formation creates the protective and decorative layer associated with the paint. The solvent evaporation rate also impacts drying time. Faster evaporation leads to quicker drying, which can be desirable for some applications but might cause challenges like brush marks if too rapid. Figure 3 illustrates unfavorable and favorable (after using optimal solvent value and ratio) surface film formation for sample 1 (Table 1).

Morphology assessment. The synergistic integration of energy dispersive X-ray spectroscopy (EDX) and scanning electron microscopy (SEM) constitutes a powerful analytical approach.[50] Their collaborative functionalities render them highly advantageous across diverse scientific and technological domains. Through the SEM's high-resolution imaging capabilities with the quantitative elemental analysis provided by EDX, researchers can figure out specific features or phases within the sample and accurately ascertain their elemental composition. EDX and SEM, when employed together, exhibit

complementary attributes, enhancing the overall analytical efficiency. Figure 4 illustrates SEM-EDX images and spectra for samples 1, 4, 5, 6, and 10 as detailed in Table 1. Consistent with expectations, the EDX spectra reveal the presence of Ti, Si, and Zn elements, each corresponding to distinct areas in the SEM images. This correspondence is contingent upon the presence of these elements in the paint formulation. It is noteworthy that the detection of gold (Au) in the EDX spectra signifies the surface coating of the samples with gold prior to testing. The precise comparison between Figure 4(a) and (b) elucidates distinct characteristics for samples 1 and 4, which incorporate 10 phr untreated TiO2 and treated TiO2 in the formulation (Table 1). This comparative analysis showed variations in the dispersion of TiO2 particles and the sizes of agglomerates after treatment. Figure 5 illustrates SEM images for samples 1, 4, 5, 6, 10, and the reference (lacking a self-cleaning agent), with corresponding details provided in Table 1. To facilitate a more effective comparison, all images share a consistent scale of 10 μm. As observed, the particles of all self-cleaning agents were distributed in the acrylic resin matrix properly. However, particles with the highest and lowest visibility belong to treated ZnO and treated SiO2, respectively. There are several possible reasons why treated ZnO particles have the highest visibility and treated SiO2 particles have the lowest visibility. Zinc oxide inherently has a higher electron density compared to silicon dioxide. This means ZnO interacts more strongly with the electron beam used in SEM, leading to brighter and more noticeable signals in the image. In addition, if the treatment roughened the surface of the ZnO particles, it can increase the surface area interacting with the electron beam, again leading to higher brightness and visibility. Even if the individual particles have similar electron density, their distribution and tendency to agglomerate can affect their visibility in the SEM image. Tightly packed or agglomerated particles might appear less distinct compared to more evenly dispersed ones. Also, charging can occur during SEM imaging, especially for SiO2. This can distort the image and further reduce the visibility of the particles.

Hydrophilic, hydrophobic, and self-cleaning property assessment. Figure 6 illustrates typical contact angles (θ) between a droplet of water and formulated paints, Samples 11 and 6 (Table 1). Table 2 presents the contact angles (θ) observed between a droplet of water and automotive oil on paints formulated with various amounts of self-cleaning agents as detailed in Table 1. The reference compound (RC) is a baseline containing acrylic resin without self-cleaning agents, TiO2, SiO2, and ZnO. Notably, with the exception of Sample 12, the water contact angles for all paints incorporating self-cleaning agents were lower than the RC value of 100°. This indicates an enhancement in the hydrophilic properties of the paints following the addition of the specified agents to the paint formulation. Water contact angles ranged from 68° for Sample 10 (with 5, 2.5, and 2.5 phr treated TiO2, SiO2, and ZnO) to 97° for Sample 2 (with 10 phr untreated SiO2). A similar trend, excluding Sample 8 with equivalent amounts of treated TiO2, SiO2, and ZnO in the formulation, was observed for the oil contact angle in paints with incorporated self-cleaning agents. The oil contact angle for RC was 33°, while it ranged from 27° for Samples 1, 10, and 11 to 33° for Sample 5 with 10 phr treated SiO2 in the formulation. The corresponding value for Sample 8 was 42°. As a general conclusion, self-cleaning agents in paint formulation improved both water and oil absorption. However, few exceptions suggest complex interactions between agents.

Figures 7 and 8 depict the qualitative self-cleaning characteristics of selected samples, denoted as RC (a and b), 2 (c and d), 8 (o and p), 10 (k and l), and 12 (I and j), as elaborated in Table 1, utilizing carbon black and automotive oil as potential contaminants. The images show the droplet position exactly after contact with the surface of paint and after a minute of contact. In Table 2, a subtle self-cleaning effect is observed in the RC sample with acrylic resin, devoid of any self-cleaning agents such as TiO2, SiO2, and ZnO in the formulation. The water droplet exhibits a non-complete spherical shape with a contact angle of 100° as described above, indicating a relatively hydrophilic paint surface. However, upon the application of a thin layer of carbon black and the introduction of a water droplet onto it, the slipping rate is observed to be low. Furthermore, the absorption of carbon by water and the removal of carbon black (contaminant) from the paint surface are found to be inadequate. In Figure 7 (c and d), the self-cleaning property of an untreated agent, specifically SiO2 (Sample 2, Table 1), is illustrated. While there is an improvement compared to the RC sample, it remains unremarkable. The subsequent samples, featuring various types and quantities of self-cleaning agents, exhibit superior self-cleaning properties, characterized by high water droplet slipping and efficient removal of carbon black. Figure 8 evaluates the aforementioned property using automotive oil as a contaminant. Notably, the water droplet for all samples, including RC, approaches a completely spherical shape, indicating water repellency of the surface. However, the slipping rate of the water droplet for RC is highest among samples with self-cleaning agents in formulations, concerning potential safety for driving on painted surfaces. The heightened slipping rate may lead to the skidding of vehicle tires because of direct contact between oil and the tire tread. Conversely, the slipping rate of water droplets is significantly lower for samples with self-cleaning agents, particularly for treated agents. With the exception of RC, the water droplet carries a little oil during slipping, signifying a positive attribute for the self-cleaning property of the paint surface. In conclusion, the effectiveness of self-cleaning paints depends on an interplay of surface properties, the type and amount of self-cleaning agents used, and the nature of the contaminants. By understanding these mechanisms, researchers can design paints with better self-cleaning performance and ensure their safety for practical applications.

Conclusions

From this study it was concluded that heat treatment (800°C) of TiO2 improved crystallinity and removed impurities, leading to higher peak intensities in FT-IR and XRD. However, crystallite size reduction might have contributed to decreased peak intensities in XRD. For SiO2, heat treatment induced phase transformation to quartz, resulting in stronger peaks in XRD. It

also removed water molecules and impurities, contributing to peak intensity changes in FT-IR. Also, high-temperature treatment promoted crystal growth and densification, potentially affecting peak intensities in both FT-IR and XRD for ZnO. Subtle changes in Zn-O bond configuration could also contribute to FT-IR peak intensity changes. The solvent ratio and amount significantly impacted paint viscosity and drying time. SEM-EDX analysis confirmed the presence and distribution of self-cleaning agents in the paint matrix. Treated ZnO particles had the highest visibility in SEM due to higher electron density and potentially increased surface area. Treated SiO2 particles had the lowest visibility due to lower electron density, potential agglomeration, and charging during imaging. Self-cleaning agents generally increased both water and oil absorption compared to the reference paint. The qualitative assessment confirmed superior self-cleaning performance for paints with self-cleaning agents compared to the reference paint, especially for treated agents. The water droplet slipping rate on oil-contaminated surfaces was highest for the reference point, raising safety concerns. Overall, modifying self-cleaning agents with heat treatment can influence their properties, potentially impacting their effectiveness in paint formulations. The type and amount of self-cleaning agents significantly affect the hydrophilicity, hydrophobicity, and self-cleaning performance of paints. Balancing these properties with safety considerations is crucial for practical applications.

Acknowledgments

The SEM, XRD, EDX, and FT-IR experiments were performed in the central laboratory, faculty of science, and research laboratory for industrial catalysis and environment of the Ferdowsi University of Mashhad. The authors thank the laboratory staff for their sincere cooperation.

Author Contributions

Hoora Shahgolzade, and Saeed Ostad Movahed designed the experiments. Dr Saeed Ostad Movahed prepared the manuscript with contributions from all co-authors. The authors applied the SDC approach for the sequence of authors.

Declaration of conflicting interests

The author(s) declared no potential conflicts of interest with respect to the research, authorship, and/or publication of this article.

Funding

The author(s) received no financial support for the research, authorship, and/or publication of this article.

ORCID iD

Saeed Ostad Movahed https://orcid.org/0000-0002-2743-5739

Data availability Statement

The datasets generated during and/or analyzed during the current study are available from the corresponding author upon reasonable request.

References

1. Taheri M, Jahanfar M and Ogino K. Synthesis of acrylic resins for high-solids traffic marking paint by solution polymerization. *Des Monomers Polym* 2019; 22(1): 213–225.
2. Ito T, Tohriyama K and Kamata M. Detection of damaged road paints of crosswalks by focusing on multi-layered features. *Int J Automot Eng* 2019; 10(4): 356–364.
3. Eriskin E, Karahancer S, Terzi S, et al. Increasing the visibility of roads using phosphorous paint. *Road Mater Pavement Des* 2019; 20(1): 199–210.
4. Xu L, Chen Z, Li X, et al. Performance, environmental impact and cost analysis of marking materials in pavement engineering, the-state-of-art. *J Clean Prod* 2021; 294: 126302.
5. Moghadam SG, Pazokifard S and Mirabedini SM. Silane treatment of drop-on glass-beads and their performance in two-component traffic paints. *Prog Org Coating* 2021; 156: 106235.
6. Tayebi M, Ostad Movahed S and Ahmadpour A. The effect of the surface coating of a strontium mono-aluminate europium dysprosium-based (SrAl 2 O 4: Eu 2+, Dy 3+) phosphor by polyethylene (PE), polystyrene (PS) and their dual system on the photoluminescence properties of the pigment. *RSC Adv* 2019; 9(66): 38703–38712.
7. Jaberi F, Movahed SO and Ahmadpour A. The study on titanium dioxide-silica binary mixture coated SrAl 2 O 4: Eu 2+, Dy 3+ phosphor as a photoluminescence pigment in a waterborne paint. *J Fluoresc* 2019; 29: 461–471.
8. Taheri M, Jahanfar M and Ogino K. Wear properties of nanocomposite traffic marking paint. *J Nanomater* 2018; 2: 1.
9. Babić D, E Burghardt T and Babić D. Application and characteristics of waterborne road marking paint. *International Journal for Traffic and Transport Engineering* 2015; 5(2): 150–169.
10. Gurgone N, Miliani C and Moretti P. *Chapter eighteen chlorinated rubber paint film*. Conservation Issues in Modern and Contemporary Murals, 2015, 285.
11. Haider AJ, Jameel ZN and Al-Hussaini IH. Review on: titanium dioxide applications. *Energy Proc* 2019; 157: 17–29.
12. Otterstedt JE, Otterstedt JE, Brandreth DA, et al. Pigments. In: *Small particles technology*, 1998, pp. 369–405.

13. Sun D and Zhang Y. Preparation of fast-drying waterborne nano-complex traffic-marking paint. *J Coat Technol Res* 2012; 9: 151–156.
14. Burghardt T, Pashkevich A and Żakowska L. Contribution of solvents from road marking paints to tropospheric ozone formation. *Bud-Arch* 2016; 15(1): 7–18.
15. Mazzoni LN, Machado DD, Vasconcelos KL, et al. Characterization of glass beads by image methods for pavement marking retroreflectivity. *Transportes* 2022; 30(2): 2584.
16. Taheri M, jahanfar M and Ogino K. Self-cleaning traffic marking paint. *Surface Interfac* 2017; 9: 13–20.
17. Xu F, Wang T, Chen H, et al. Preparation of photocatalytic TiO2-based self-cleaning coatings for painted surface without interlayer. *Prog Org Coating* 2017; 113: 15–24.
18. Rocha Segundo I, Ferreira C, Freitas EF, et al. Assessment of photocatalytic, superhydrophobic and self-cleaning properties on hot mix asphalts coated with TiO2 and/or ZnO aqueous solutions. *Construct Build Mater* 2018; 166: 500–509.
19. Osburn L. Literature review on the application of titanium dioxide reactive surfaces on urban infrastructure for depolluting and self-cleaning applications, 2008.
20. Sassoni E, D'Amen E, Roveri N, et al. Durable self-cleaning coatings for architectural surfaces by incorporation of TiO2 nano-particles into hydroxyapatite films. *Materials* 2018; 11(2): 177.
21. Rocha Segundo I, Freitas E, Landi S Jr, et al. Smart, photocatalytic and self-cleaning asphalt mixtures: a literature review. *Coatings* 2019; 9(11): 696.
22. Lu C, Zheng M, Liu J, et al. Characterization of self-cleaning pavement coatings with catalytic-hydrophobic synergistic effects. *Construct Build Mater* 2023; 397: 132246.
23. Aalto-Korte K. *Acrylic resins. Kanerva's occupational dermatology*. Switzerland: Springer Nature, 2020, pp. 737–756.
24. Sun C, Dai J, Zhang H, et al. Preparation and characterization of spherical titania and their influence on self-cleaning and anticorrosion properties of acrylic resin. *Prog Org Coating* 2019; 128: 21–31.
25. Sawada T, Sawada T, Kumasaka T, et al. Self-cleaning effects of acrylic resin containing fluoridated apatite-coated titanium dioxide. *Gerodontology* 2014; 31(1): 68–75.
26. Pal S, Contaldi V, Licciulli A, et al. Self-cleaning mineral paint for application in architectural heritage. *Coatings* 2016; 6(4): 48.
27. Guo MZ, Maury-Ramirez A and Poon CS. Self-cleaning ability of titanium dioxide clear paint coated architectural mortar and its potential in field application. *J Clean Prod* 2016; 112: 3583–3588.
28. Pawar SS, Baloji Naik R, Rath SK, et al. Photoinduced hydrophilicity and self-cleaning characteristics of silicone-modified soya alkyd/TiO 2 nanocomposite coating. *J Coat Technol Res* 2020; 17: 719–730.
29. Stieberova B, Zilka M, Ticha M, et al. Application of ZnO nanoparticles in a self-cleaning coating on a metal panel: an assessment of environmental benefits. *ACS Sustainable Chem Eng* 2017; 5(3): 2493–2500.
30. Chen MC, Koh PW, Ponnusamy VK, et al. Titanium dioxide and other nanomaterials based antimicrobial additives in functional paints and coatings: review. *Prog Org Coating* 2022; 163: 106660.
31. Ng PP. *Preliminary study of self-cleaning coating by applying nano titanium dioxide additive/Ng Pui Pui (Doctoral dissertation)*. (University of Malaya), 2015.
32. Saad SR, Mahmed N, Abdullah MMAB, et al. Self-cleaning technology in Fabric: a review. *IOP Publishing* 2016; 133(1): 012028.
33. Mendoza AI, Moriana R, Hillborg H, et al. Super-hydrophobic zinc oxide/silicone rubber nanocomposite surfaces. *Surface Interfac* 2019; 14: 146–157.
34. Cheng H, Wang F, Ou J, et al. Solar reflective coatings with luminescence and self-cleaning function. *Surface Interfac* 2021; 26: 101325.
35. Parimalam M, Islam MR and Yunus RM. *Effects of nanosilica, zinc oxide, titatinum oxide on the performance of epoxy hybrid nanocoating in presence of rubber latex Polymer Testing*, 2018, vol 70, pp. 197–207.
36. Islam MR, Parimalam M, Sumdani MG, et al. Rheological and antimicrobial properties of epoxy-based hybrid nanocoatings. *Polym Test* 2020; 81: 106202.
37. Parimalam M, Islam MR and Yunus RM. Effects of nano- and micro-sized inorganic filers on the performance of epoxy hybrid nanocoatings. *Polym Polym Compos* 2019; 27(2): 82–91.
38. Parimalam M, Islam MR and Yunus RM. Effects of nanosilica and titanium oxide on the performance of epoxy–amine nanocoatings. *J Appl Polym Sci* 2019; 136: 47901.
39. Parimalam M, Islam MR, Yunus R, et al. Effects of Colloidal nanosilica on epoxy-based nanocomposite coatings. *Progress in Color, Colorants and Coatings* 2019; 12(2): 71–82.
40. Saleh NS, Ostad Movahed S and Attarbashi F. Study on the anti-biofouling effects of the grafted polyamide 6 fibers by several vinyl chemicals. *J Appl Polym Sci* 2018; 135(42): 46760.
41. https://prideinstrument.en.made-in-china.com/productimage/QyFJekAZhEhp2f1j00sASTKPEanDqj/China-Lab-Equipment-4-Side-Paint-Film-Applicator-for-Painting.html
42. Guo Q, Zhou C, Ma Z, et al. Fundamentals of TiO2 photocatalysis: concepts, mechanisms, and challenges. *Adv Mater* 2019; 31(50): 1901997.
43. Su W, Zhang J, Feng Z, et al. Surface phases of TiO2 nanoparticles studied by UV Raman spectroscopy and FT-IR spectroscopy. *J Phys Chem C* 2008; 112(20): 7710–7716.
44. Prasad K, Pinjari DV, Pandit AB, et al. Phase transformation of nanostructured titanium dioxide from anatase-to-rutile via combined ultrasound assisted sol–gel technique. *Ultrason Sonochem* 2010; 17(2): 409–415.
45. Swann GE and Patwardhan SV. Application of Fourier Transform Infrared Spectroscopy (FTIR) for assessing biogenic silica sample purity in geochemical analyses and palaeoenvironmental research. *Clim Past* 2011; 7(1): 65–74.

46. Nabil M, Mahmoud KR, El-Shaer A, et al. Preparation of crystalline silica (quartz, cristobalite, and tridymite) and amorphous silica powder (one step). *J Phys Chem Solid* 2018; 121: 22–26.
47. Reddy BM, Khan A, Lakshmanan P, et al. Structural characterization of nanosized CeO2− SiO2, CeO2− TiO2, and CeO2− ZrO2 catalysts by XRD, Raman, and HREM techniques. *J Phys Chem B* 2005; 109(8): 3355–3363.
48. Xiong G, Pal U, Serrano JG, et al. Photoluminesence and FTIR study of ZnO nanoparticles: the impurity and defect perspective. *Phys Status Solidi* 2006; 3(10): 3577–3581.
49. Singh P, Kumar A, Kaushal A, et al. In situ high temperature XRD studies of ZnO nanopowder prepared via cost effective ultrasonic mist chemical vapour deposition. *Bull Mater Sci* 2008; 31: 573–577.
50. Abd Mutalib M, Rahman MA, Othman MHD, et al. Scanning electron microscopy (SEM) and energy-dispersive X-ray (EDX) spectroscopy. *Membrane characterization* 2017; 3: 161–179. Elsevier.